

# EVOLUTION OF STRUCTURE OF OXIDE DISPERSION STRENGTHENED NICKEL ALLOYS IN FUSION WELDING

K.A. YUSHCHENKO, B.A. ZADERY, I.S. GAKH,  
A.V. ZVYAGINTSEVA, L.M. KAPITANCHUK and Yu.V. KHASKIN  
E.O. Paton Electric Welding Institute of the NAS of Ukraine  
11 Kazimir Malevich Str., 03150, Kyiv, Ukraine. E-mail: [office@paton.kiev.ua](mailto:office@paton.kiev.ua)

Changes of nanodispersed structure of nickel ODS-alloys as a result of fusion welding were considered. Welded joints, produced at different modes of argonarc, electron beam and laser welding were investigated. It is shown that degradation of nanosized structure takes place in all considered cases. It is expressed mainly in change of strengthening particles up to micro-sized level, some variation of their chemical composition and morphology. A level of structure degradation depends on a level of overheating of weld pool metal, which in turn, is determined by value of specific power of heat source, welding rate, heat input and cooling nature. It is shown that the positive result, i.e. minimum degradation of initial metal nanostructure, can be reached at optimum combination of the maximum technologically acceptable welding rate and heat input concentration, minimum margin and controlled distribution of power, which provide through penetration and formation of weld with parallel fusion surfaces. 19 Ref., 9 Figures.

**Keywords:** ODS-nickel alloys, fusion welding, weld pool, degradation of nanodispersed structure, particle coarsening, welding rate, heat input nature, weld formation

Oxide dispersion strengthened nickel alloys and steels due to combination of unique properties exceeding characteristics of the materials strengthened by micron size particles [1–9] recently find more and more application as alternative structural material in perspective developments of nuclear mechanical engineering, aerospace equipment, energy generating branches, including renewable power sources, high-temperature heat exchangers, engine construction etc. [2, 10–13].

The main problem that should be solved for realizing the properties of these materials in industrial structures is to guarantee nanodimension structure during the whole process chain of their manufacture. The main characteristics of such a structure is size of the strengthening particles, their morphology, composition, uniformity of distribution in matrix.

The particular difficulty for performance of this task during welding lies in high-temperature heating of metal, nonequilibrium of thermal, hydrodynamic, thermal deformation, solidification and other processes accompanying formation of welded joint.

Probably, the maximum preservation of the parameters of ODS-alloy nanostructure in their welding is possible with using the methods eliminating or minimizing metal overheating above dissociation or melting temperature as well as oxide coagulation during joint formation. These are diffusion, friction, friction stir and other welding methods. However, they have

limitations in their realizing, it is technical impossibility of welding of structures with complex developed geometry, application of the methods under conditions of special production or repair, not proved technology and equipment. And even growing in popularity in the recent time friction stir welding method does not always allow getting quality joint and keep initial structure [14–17]. Therefore, today it is a still relevant task to weld ODS-alloys using the methods of wide commercial application, namely argonarc (ArAW), laser (LW), electron beam (EBW).

Present work was carried out using single-phase nickel alloy Inconel MA758 (Ni–31Cr–1.0Fe–0.5Ti–0.3Al–0.6Y<sub>2</sub>O<sub>3</sub>) as a model one. Such a choice was caused by the need to eliminate negative effect of phase transformations on nanostructure formation. The welded samples of 1.5–2.0 mm thickness were cut by spark method from a rod produced by mechanical alloying method. The cut places were polished, the samples were rinsed by acetone in ultrasonic pool.

Welding experiments were carried out using the methods mentioned above.

Welding rate was the main parameter used for regulation of heat input in weld metal. It allowed taking into account efficiency and mobility of impact as well as quality effect similarity on nature of heat input and weld pool hydrodynamics at different fusion welding methods. During the experiments the welding rate was

varied in a wide range of values from 12 to 180 m/h. The values of other mode parameters were selected based on the need of achievement of through penetration and quality formation of the weld. It should be underlined that a significant difference of thermophysical characteristics of oxides and base metal (such as specific weight, melting temperature, oxides' wetting, etc.) considerably complicates quality formation of the welds. It is shown by undercuts, spattering, blowing-out and splashes of metal, floating of oxides, appearance of porosity and other defects.

This is particularly obvious in welding at low rates. Weld metal, produced at 10–20 m/h rates, differs by insufficient mixing, structural and chemical inhomogeneity, considerable coarsening and loss of nanosized oxides (Figure 1).

Therefore, the main metal physical investigations were carried out on optimally formed welds produced at high welding rates (Figure 2). At that it was reasonable to use maximum amount of the samples to cover different heat input variants. The welding modes corresponded to overrated (EBW, 90 m/h), optimum (LW, 90 m/h) and underrated (LW 180 m/h) heat input. EBW produced welds (90 m/h, 2.8 kW) due to overrated melt volume corresponded to heat transfer mainly through weld pool melt surface and significant overheating, and based on this index were approximated to the welds made by ArAW. The welds, produced by LW at 90 m/h rate, due to presence of open weld pool keyhole, were subjected to less overheating in contrast to welds made by LW at 180 m/h rate, where heat transfer was performed through side walls of the keyhole, mirror and weld pool bottom. Effect of heat input excess in the latter case was compensated due to increase of welding rate.

Nature of the heat input can be estimated following the analysis of dimensions and geometry of welds (Figure 2).

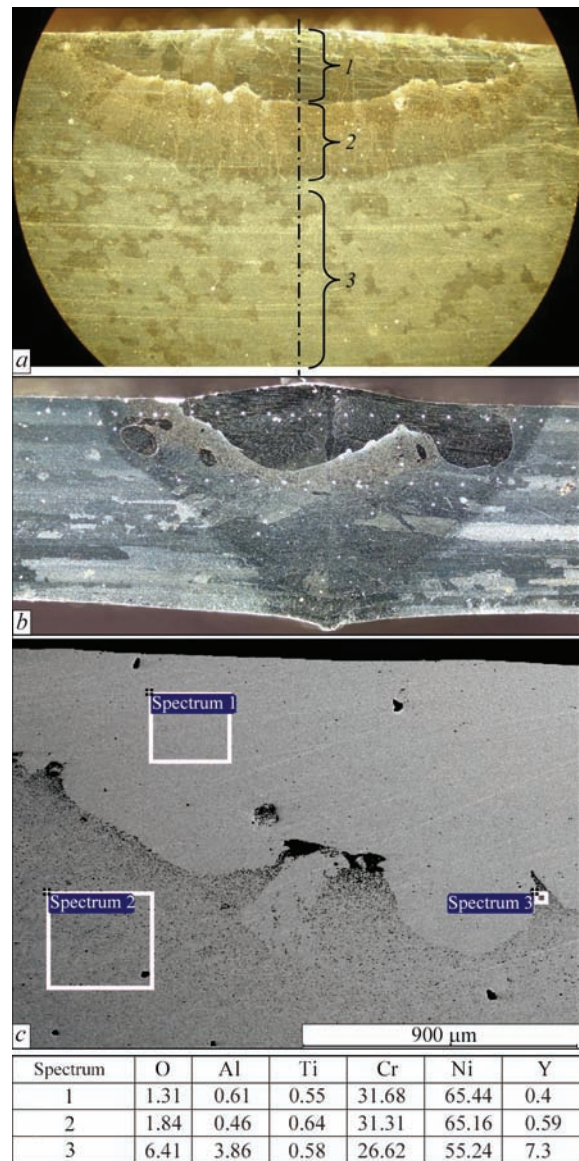


**Figure 1.** Macrostructure (*a* —  $\times 40$ ; *b* —  $\times 50$ ) of welded joint produced by ArAW: *a* — surface fusion of massive sample,  $v_w = 8$  m/h ( $1 - 0.1Y_2O_3$ ;  $2 - 0.47Y_2O_3$ ;  $3 - 0.57Y_2O_3$ ); *b* — sample of 2 mm thickness,  $v_w = 16$  m/h; *c* — section of weld *b* and its element-by-element analysis, at. %

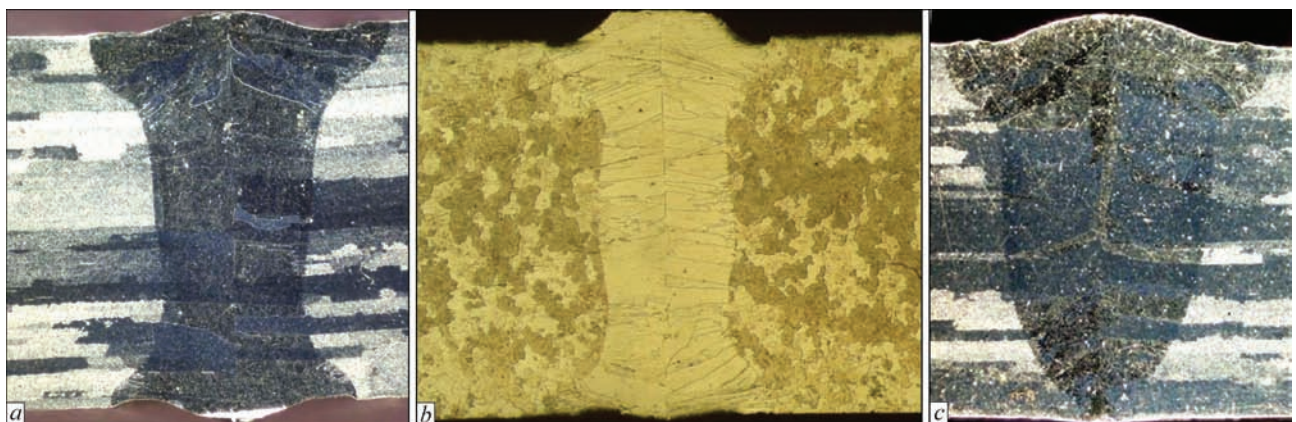


**Figure 2.** Macrosections ( $\times 30$ ) of examined welded joints from alloy InMA758: *a* — EBW,  $v_w = 90$  m/h, overrated beam power 2.8 kW; *b* — LW,  $v_w = 90$  m/h, beam power 2.2 kW; *c* — LW,  $v_w = 180$  m/h, beam power 2.2 kW

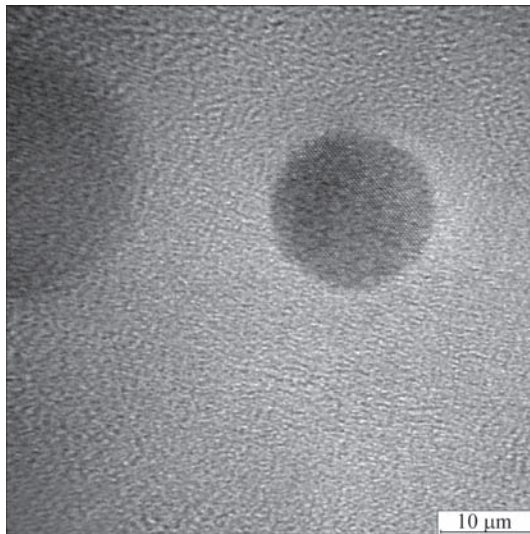


**Figure 3.** Transmission microscopy of initial metal of alloy InMA758 (photo was made in the Institute of Materials Science of the NAS of Ukraine)

Presence, size, distribution in weld metal, change of morphology and composition of strengthening nanoparticles were determined using Auger mi-

croprobe JAMP-9500F of JEOL Company (Japan) equipped with energy-dispersion X-ray spectrometer INCAP Penta FETX3 (INCA 350 system) of Oxford Instruments Company (Great Britain). At that the particles of minimum size up to 10 nm were determined.

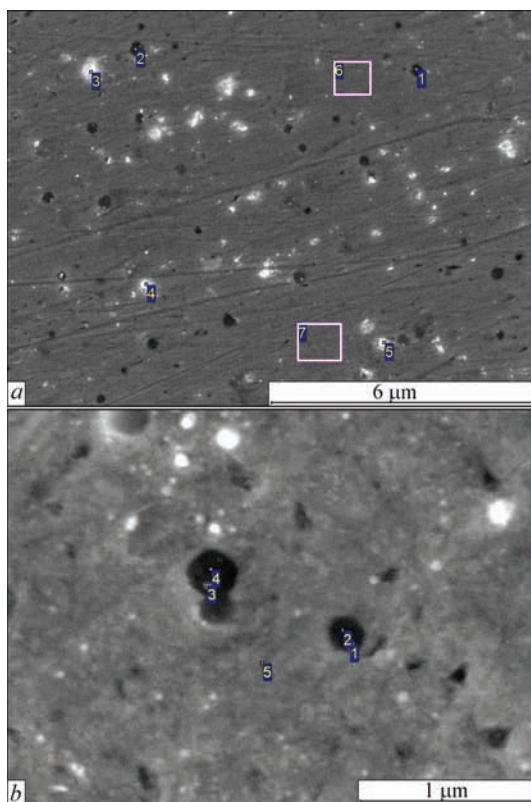
Higher accuracy on peculiarities (size, morphology, composition) of the nanoparticles can be obtained only based on the results received using transmission (Figure 3) or atomic-force microscope. However, it provokes problems with correct interpreting of the results received from some areas of the welded joint.

Taking into account indicated difficulties, quality picture of total distribution and presence of precipitations of different dispersion were evaluated following the analysis of dark-field optical images of the microstructure. They demonstrate obvious image contrast due to differences of physicomechanical properties of the strengthening particles and metal matrix (Figure 4).

Analysis of the examination results shows that structure of initial material in as-delivered condition is characterized with noticeable inhomogeneity on



**Figure 4.** Microstructure (*a* —  $\times 200$ ; *b-d* —  $\times 500$ ) of welds (photo in dark field): *a* — transition area «heat affected zone–weld metal», LW,  $v_w = 90$  m/h; *b* — weld metal, EBW,  $v_w = 90$  m/h; *c* — weld metal, LW,  $v_w = 90$  m/h; *d* — weld metal, LW,  $v_w = 180$  m/h



Spectrum	C	N	O	Al	Si	Ti	Cr	Fe	Ni	Y
1	2.74	32.88	0	0.84	0	29.02	9.94	0	23.82	0.77
2	2.43	30.40	6.61	0.46	0.41	30.54	8.89	0	20.26	0
3	1.78	0	27.43	14.02	0	0	16.54	0	40.23	0
4	2.10	0	22.26	13.09	0.25	1.03	20.61	0	40.19	0.47
5	6.57	0.63	23.44	13.16	0.35	0.50	13.37	0.54	39.76	1.67
6	3.62	0	1.97	0.33	0.29	0	28.00	1.72	63.84	0.21
7	1.69	0	3.49	0.23	0.11	0.84	29.04	0	64.60	0

Spectrum	C	N	O	Al	Ti	Cr	Fe	Ni	Y
1	5.50	22.22	5.66	0.82	24.78	12.96	0.40	26.73	0.94
2	4.57	19.69	1.16	0.41	27.34	15.10	0	31.49	0.24
3	3.98	30.58	0	0.64	30.39	11.26	0	22.60	0.56
4	3.94	31.93	0.66	0.28	31.73	8.41	0.80	22.06	0.20
5	4.45	1.23	2.69	0.35	0	25.50	1.15	64.17	0.47

**Figure 5.** Electron image of microstructure and analysis of chemical composition, at.%: *a* — initial metal; *b* — base metal

size as well as precipitation composition (Figures 4, 5). More than 10 different types of precipitations were found. The most typical among them are:

- nanosized oxygen-containing of Y–O–, Al–O, Y–Al–O type make around 80 % of all detected, around 30 % of which are referred to precipitations of complex type Y–Al–O;

- microsized nitrogen-containing of Ti–C–N, Ti–N type make approximately 20 %.

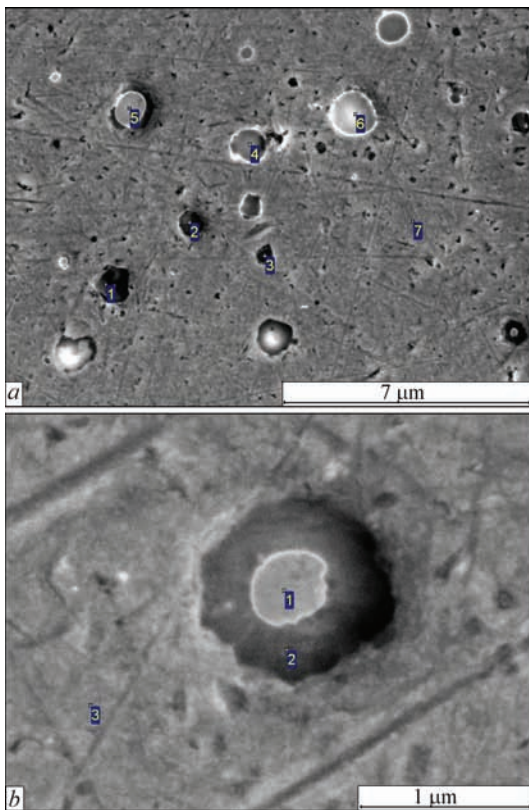
It should be underlined that around 25 % of oxygen-containing nanoparticles are located in the center or along the surface of nitrogen-containing precipitations (Figure 5), size of the latter can make from 140 to 630 nm. Therefore, results of their energy-dispersion analysis (EDA) often demonstrate presence of nitrogen, carbon, iron and other alloy components.

The main mass of precipitations is nanosized particles (around 15–30 nm), which mainly cause ODS-alloys specific properties [1–9] due to high specific surface energy and high resistance to dislocation displacement. Less part is microsized precipitations (around 110–290 nm), main role of which most likely comes to increase of strength according to classical theory of dispersion strengthening [18, 19]. There are also separate precipitations of different composition of around 600–1200 nm size as well as conglomerates of nanosized particles of area approximately 200–4000 nm<sup>2</sup> and more (Figure 5).

In process of welding, regardless high rates of its performance and apparent small overheating, alloy microstructure is subjected to significant changes. Size, morphology and composition of the main strengthening constituents (Figures 6–8) are changed. Virtually in all considered cases the size of oxygen-containing precipitations of Y–Al–O type rises 2–5 times at significant decrease of size and content of Y–O and Al–O precipitations. Nitrogen-containing precipitations of Ti–N and Ti–C–N type are subjected to lower changes. Oxygen-containing particles of globular type, which are located inside nitrogen-containing precipitations (Figures 6–8), are found most often.

More significant changes of structure (Figure 6) are observed in the welds produced with overrated EBW heat input. As it was mentioned, the welds produced at lower rates of EBW and ArAW were eliminated from consideration due to large loss of oxides provoked by weld pool metal overheating.

LW results in increase (to 80 %) of portion of found oxide inclusions with coarse size nanoparticles up to 44–110 nm (15–24 nm in the initial metal), that, apparently, is caused by coagulation of smaller particles. Increase of microsized precipitations up to 300–510 nm (at 140–300 nm in initial metal) is noted. Portion of nitrogen-containing precipitations somewhat reduces (approximately 2–3 %). Their size rises from initial 140–290 nm to 270–410 nm and 310–410 to 600–900 nm for rare microprecipitations. Increase



Spectrum	C	N	O	Al	Ti	Cr	Fe	Ni	Y
1	2.25	47.85	0	0	35.02	9.18	0.37	5.20	0.14
2	2.71	42.76	11.43	4.52	24.07	6.02	0	3.69	4.80
3	0.54	0	55.40	15.48	1.08	4.10	0.11	8.04	15.25
4	1.50	0	58.73	16.76	1.26	1.84	0	4.17	15.74
5	2.45	0	59.19	15.70	5.14	1.28	0	1.75	14.48
6	2.99	0	60.02	16.95	1.10	0.65	0	1.38	16.92
7	2.50	0	0	0.71	0.37	28.78	0.73	66.67	0.23

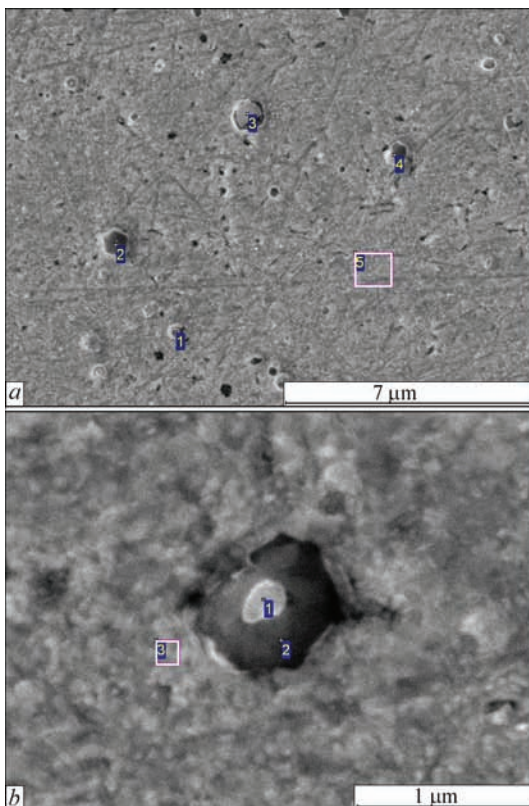
Spectrum	C	N	O	Al	Ti	Cr	Fe	Ni	Y
1	2.68	5.97	53.56	16.70	2.56	0.92	0.50	1.28	15.83
2	2.38	35.66	11.74	4.08	27.86	7.13	0	8.47	2.68
3	2.91	0.47	0	0.11	0.48	29.67	0	66.12	0.24

**Figure 6.** Electron image of microstructure and analysis of chemical composition (at.%) of weld metal (*a, b*) produced at EBW,  $v_w = 90$  m/h

of precipitation size is already noticeable on optical images in the dark field (Figure 4).

LW provokes somewhat smaller level of rise of precipitation size (Figures 7, 8) that is, apparently,

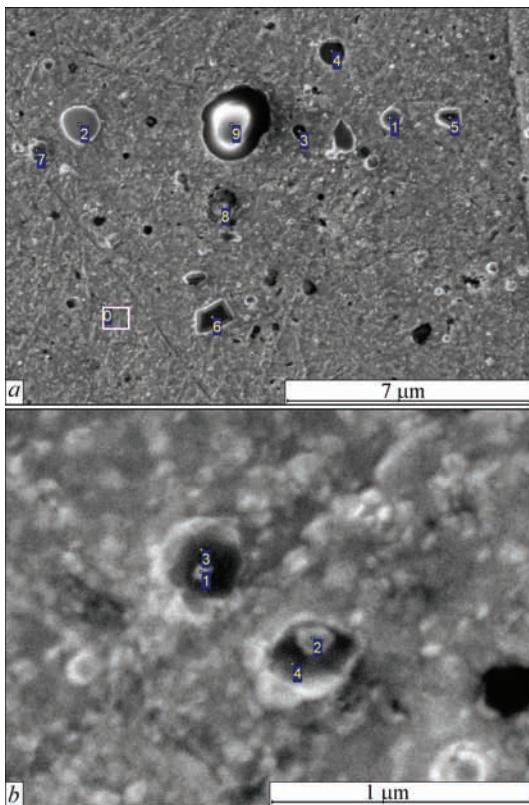
caused by increase of specific power and additional cooling due to shielding gas blowing. Thus, there is increase of size of oxygen-containing nanoparticles to 24–92 nm (Figure 7) and microsized precipitations



Spectrum	C	N	O	Al	Ti	Cr	Fe	Ni	Y
1	3.16	0	24.23	6.45	4.97	18.10	0.77	35.06	7.27
2	3.05	41.50	0	0.10	29.61	10.40	0.85	14.37	0.12
3	1.30	0	59.10	13.80	2.73	1.83	0	3.85	17.39
4	3.35	17.83	1.35	0	14.28	21.77	0	41.42	0
5	2.89	0	0.16	0.46	0.42	28.94	0	67.14	0

Spectrum	C	N	O	Al	Ti	Cr	Fe	Ni	Y
1	1.55	5.50	53.20	17.35	2.33	1.17	0.49	2.19	16.24
2	2.83	27.79	24.36	8.50	18.09	5.71	0	4.91	7.82
3	4.80	2.71	0	0.48	0.46	26.25	0.98	63.92	0.40

**Figure 7.** Electron image of microstructure and analysis of chemical composition (at.%) of weld metal (*a, b*) produced at LW,  $v_w = 90$  m/h



Spectrum	C	N	O	Al	Ti	Cr	Fe	Ni	Y
1	0.89	0	13.20	7.39	1.71	18.29	0.24	40.04	18.23
2	0.95	0	26.00	10.08	3.14	4.79	1.04	6.96	47.05
3	1.38	0	24.69	13.23	2.48	5.31	0.19	18.4	34.25
4	0.92	0	30.21	16.80	1.89	3.91	0	9.75	36.40
5	0.84	0.48	16.80	10.22	4.34	18.22	0	29.54	19.56
6	0.69	0	27.45	27.45	4.40	2.92	0.59	8.50	40.35
7	1.01	8.96	3.68	3.68	19.58	20.48	1.21	37.54	5.56
8	0.82	0	26.90	26.90	5.85	3.93	0	9.10	42.37
9	0.83	0	30.82	30.82	2.53	1.63	0	1.87	45.22
0	1.12	1.32	0	0	0	28.71	1.51	67.15	0

Spectrum	C	N	O	Al	Ti	Cr	Fe	Ni	Y
1	2.81	16.12	1.80	0.98	17.83	26.22	0	33.95	0.28
2	2.38	24.37	3.53	1.24	16.85	22.42	0	28.47	0.73
3	4.18	21.61	0	0.26	11.42	24.70	0	37.83	0
4	3.75	17.40	0	0.08	10.35	25.95	0	42.41	0.04

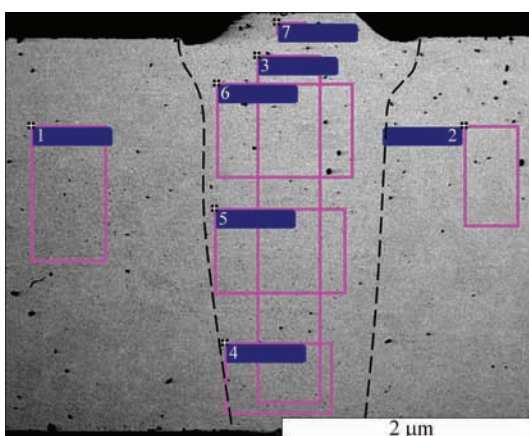
**Figure 8.** Electron image of microstructure and analysis of chemical composition (at.%) of weld metal (a, b) produced at LW,  $v_w = 180$  m/h

to 180–360 nm in the welds made at 90 m/h welding rate. Therefore, rise of size of nanoparticles to 21–70 and 140–600 nm for microsized ones takes place in the welds produced by LW at 180 m/h rate (Figure 8). Changes of nitrogen-containing precipitations are less noticeable.

As can be seen, the difference in change of precipitation sizes in the welds, made at 90 and 180 m/h rate is less obvious that indicates approximately similar level of their overheating.

At that, general for all considered cases is transformation of simple oxygen-containing phases of Y–O type into more complex Y–Al–O precipitations.

It should be noted that changes that takes place at different methods and modes of welding are less noticeable in comparison with transfer from base to weld metal. Changes in the structure, which take place as a result of welding, as it was mentioned earlier, are determined by value of weld pool metal overheating. The latter depends not only on effective power of heat source, level of its concentration, welding rate, but to significant extent on nature of heat transfer, which is determined by relationship of welding mode parameters. Thus, there is obvious difference in formation of EBW and LW weld metal structure at similar welding rate, but various effective powers and heat input nature.



Spectrum	O	Al	Ti	Cr	Ni	Y
1		0.41	0.59	31.73	66.7	0.33
2	1.66	0.4	0.52	30.96	66.46	
3		0.44	0.51	31.93	66.88	0.24
4		0.49	0.52	32.34	66.37	0.28
5		0.5	0.5	31.92	66.75	0.34
6		0.46	0.51	31.55	66.92	0.28
7		0.42	0.53	31.38	67.20	0.46
max	1.66	0.5	0.59	32.34	67.20	0.46
min	0	0.4	0.5	30.96	66.37	0

**Figure 9.** Macrosection and chemical composition (at.%) of separate areas of welded joint of alloy MA758 produced at EBW,  $v_w = 150$  m/h

At the same time, difference of nanodispersion of strengthening particles in the structure of weld metal produced by LW at different rates, but at somewhat different nature of heat input is less noticeable.

It should also be noted that selection of method, technological means and modes of welding determine as well uniformity of particle distribution on weld section. At low welding rate there is loss of significant portion of nanoparticles by the weld as well as their very nonuniform distribution along its section. In welding at increased rates more uniform distribution of the particles is reached (Figures 6–8), however, in this case there is some rise of their concentration in the weld upper part (Figure 9) due to removal of forming nanoparticles by molten metal flow.

Taking into account examination results it can be concluded that final recommendations on procedure of fusion welding of ODS-alloys can be made after setting a compromise between the conditions of formation of acceptable quality welds and limitations of nanostructure degradation as well as in evaluation of mechanical properties change.

## Conclusions

1. It is determined that nickel ODS-alloy Inconel MA758, produced by mechanical alloying method, is characterized by presence of more than ten types of nanosized (15–100 nm) and microsized (140–610 nm) oxygen- and nitrogen-containing precipitations, noticeable chemical and structural inhomogeneity.

2. Presence of oxides in ODS-alloys to significant extent complicates quality formation of welds in fusion welding.

3. Obvious degradation of initial nanodispersed structure takes place in welding of ODS-alloys. Complete or partial loss of oxide strengthening nanoparticles in weld metal, their significant coagulation, change of morphology and chemical composition as well as formation of new phase precipitations is observed depending on method, conditions and modes of welding.

4. Level of structure degradation is mainly determined by value of weld pool metal overheating, which depends essentially on specific power of heat source, welding rate, nature of heat input and cooling in process of welding.

5. Technologically positive result can be reached due to optimization of heat input in weld pool by

means of increase of welding rate and concentration of heat source power at minimal margin of power and its controlled distribution on weld pool section.

- Gessinger, G.Kh. (1988) *Powder metallurgy of high-temperature alloys*. Chelyabinsk, Metallurgiya, Chelyab. Div. [in Russian].
- Valiev, F.Z., Aleksandrov, I.V. (2007) *Volumetric nanostructured metallic materials: Production, structure and properties*. Moscow, IKTs Akademkniga [in Russian].
- Chebryakova, E.V. (2011) Peculiarities of mechanism of strengthening of metal matrices with nanoparticles of refractory compounds. In: *Proc. of All-Russian Conf. on Nanomaterials NANO 2011*. Moscow, IMET RAN [in Russian].
- Gusev, A.I. (1998) Effect of nanostructural state in compact metals and joints. *Uspekhi Fiz. Nauk*, **168**, 29–58 [in Russian].
- Soni, P.R. (2000) *Mechanical alloying: Fundamentals and applications*. Cambridge, Cambridge Int. Sci. Publ.
- He, X.D., Xin, Y., Li, M.W., Sun, Y. (2009) Microstructure and mechanical properties of ODS-Ni-based superalloy foil produced by EB-PVD. *J. of Alloys and Compounds*, **467**(1–2), 347.
- Gleiter, H. (2000) Nanostructured materials. Basic concepts and microstructure. *Acta Mater.*, **48**(1), 1–29.
- Andrievsky, R.A., Glezer, A.M. (1999) Size effects in nanocrystalline materials. Peculiarities of structure. *Fizika Metallov i Metallovedenie*, **88**(1), 50–73 [in Russian].
- Rebinder, P.A. (1958) *Physicochemical mechanics*. Moscow [in Russian].
- Janko, B. (1986) *High-temperature alloys for gas turbines and other application*. Brussels, D. Ridee.
- Kondrik, A.I., Kovtun, G.P., Datsenko, O.A. et al. (2008) *Modern materials for thermonuclear power engineering*. Kharkov, NNTsKhPTI [in Russian].
- Azerenkov, N.A., Kovtun, G.P., Litovchenko, S.V. (2009) Nanotechnologies and nanomaterials in nuclear power engineering. In: *Proc. of Int. Scient. Conf. on Physicochemical Principles of Formation and Modification of Micro- and Nanostructures. FMMN, Zbirnyk Nauk. Prats.* Kharkiv, NFTTsMON ta NANU, 2009, 152–157.
- Kovtun, G.P., Verevkin, A.A. (2010) *Nanomaterials: Technologies and materials science* (Review). Kharkov, NNTs KhPTI [in Russian].
- Howard, S.M., Jasthi, DB, K., Arbogast, W.J. et al. (2004) Friction stir welding of MA957 oxide dispersion strengthened ferritic steel. In: *Fusion materials semiannual progress report for the period ending. December 31*, 55–60.
- Hemilton, M.L. et al. (2000) Fabrication technology for ODS alloy MA957, PNL-13165.
- Shinozaki, K et al. (1997) Metallurgical and mechanical properties of ODS alloy MS956 friction welds. *Welding J.*, **76**(8), 289–299.
- Feng, Z., Ren, W. (2006) Initial development in joining of ODS alloys using friction stir welding. Report No. *ORNL/GEN4LTR-06-021*.
- Portnoj, K.I., Babich, V.N. (1974) *Dispersion-hardened materials*. Moscow, Metallurgiya [in Russian].
- Kelly, A., Nicholson, R. (1966) *Dispersion hardening*. Moscow, Metallurgiya [in Russian].

Received 12.04.2018